3. Results

3.1 Epithelial organization within the migratory pllp

It is a fundamental problem of developmental biology to understand how single cell behaviors affect global tissue and organ morphogenesis. One example of dynamic single cell behaviors that contribute to higher order tissue organization occurs during development of the zebrafish posterior lateral line primordium (pllp). The pllp is a small cohesive migratory epithelial tissue that produces neuromasts of the posterior lateral line organ, which are composed of sensory hair and their support cells. During migration, pllp cells form rosettes associated with Delta expression, which periodically partition from the trailing end and are deposited along the migratory path (Itoh and Chitnis, 2001; Ghysen and Dambly-Chaudiere, 2004). In this study, I investigated the subcellular dynamics underlying cellular rosette formation and, hence, morphogenesis of the posterior lateral line organ.

During migration, the pllp is comprised of approximately one-hundred cells that are organized as a compact migratory tissue (Ghysen and Dambly-Chaudiere, 2004; Haas and Gilmour, 2006). To visualize the subcellular organization of cells during rosette formation within the pllp, I performed immunohistochemical stainings at 32-36 hours post fertilization (hpf) using antibodies against the apical marker atypical protein kinase C (PRKC; formerly named aPKC), E-Cadherin, Zonula occludens-1 (ZO-1), and actin. At the leading (distal) edge of the pllp, ZO-1 was not localized whereas E-Cadherin and PRKC were distributed among all intercellular membranes (Figure 3A,C). Similarly, actin was localized to intercellular membranes but highly enriched within spotted apical bands along anterior-posterior interfaces (see white arrowheads in Figure 3B). γ-tubulin-positive centrosomes were randomly distributed within the plane of the epithelium (Figure 3D). Towards the trailing (proximal) edge, the pllp displayed 2-3 cellular rosettes. Within rosettes, cells exhibited apical ZO-1, PRKC and actin rich focal points and acquired bottlenecked shapes (Figure 3A-C). Throughout

the entire pllp, E-Cadherin was uniformly localized among all intercellular membranes and was not enriched within apical focal points. Three-dimensional reconstructions of confocal z-stack images revealed that apical focal points were associated with presumptive hair cells that were positioned below the plane of the epithelial layer. These presumptive hair cells were recognized by the deep nuclear label (see white asterisks within red and green insets in Figure 3A,B) and by Delta D expression (see below). Consistent with a strong polarization of rosette cells, centrosomes were localized close to the apical side whereas nuclei were localized to the opposite basal sides of rosette cells (Figure 3D). Individual rosettes were surrounded by presumptive inter-neuromast cells.

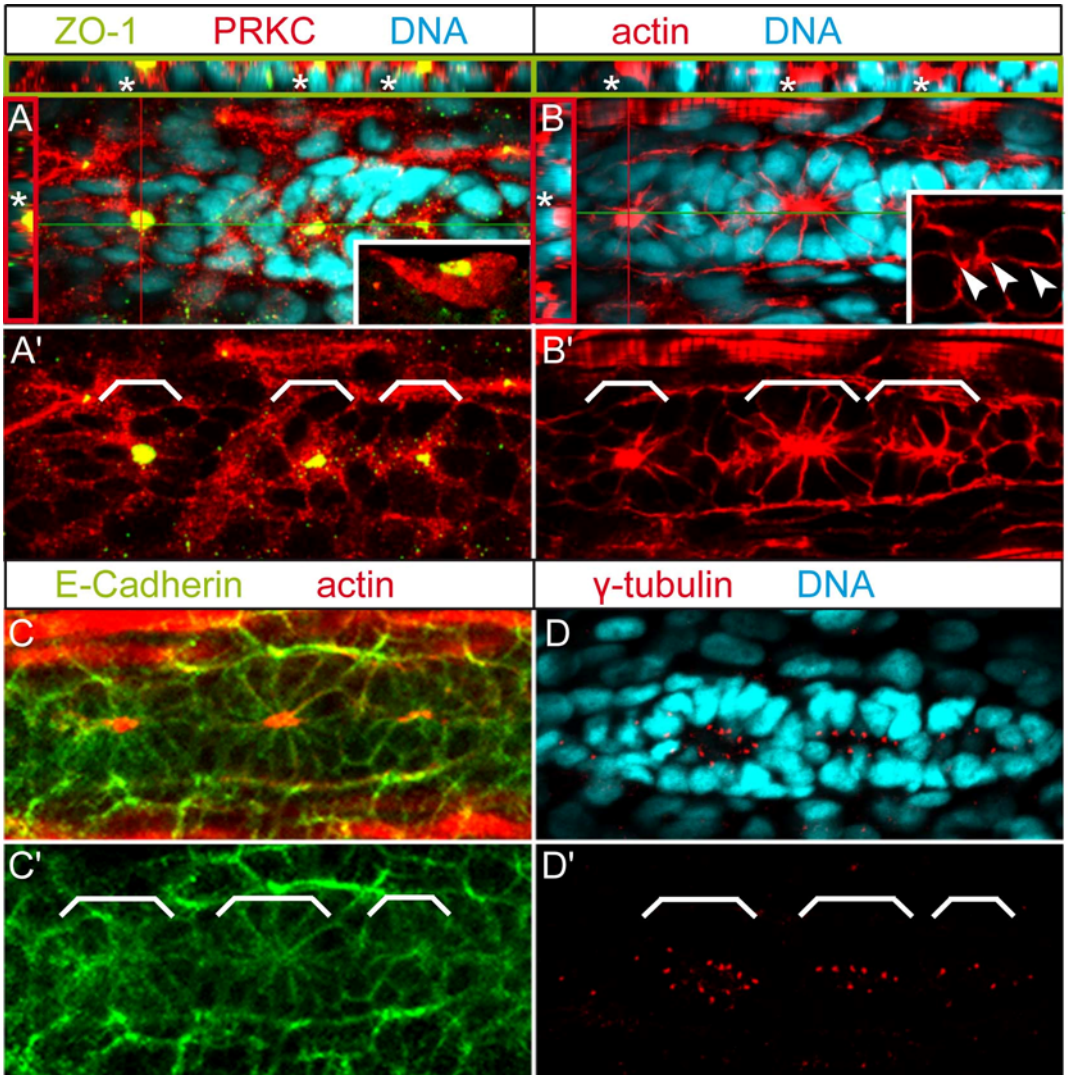

Figure 3: Epithelial organization and apical membrane constriction during pllp rosette formation. Epithelial organization of pllp cells was assayed by immunohistochemistry. Shown are reconstructions of confocal images of the pllp at 36 hpf. (A,B) Red lines indicate cross section planes, green lines sagital section planes and the respective sections are shown within red (apical to the left) or green insets (apical to the top). White brackets indicate position of individual rosettes. Cross and sagital sections reveal that ZO-1 and actin rich constrictions are apical and single presumptive hair cells are below the plane of the epithelial layer (recognized by the deep nuclear staining, indicated by white asterisks). (A) White inset shows transverse section of the pllp. (B) White inset shows details of the leading edge region, which contains apical actin spots along anterior-posterior interfaces (white arrowheads). Dynamic apical constriction of actin and apical ZO-1 localization occur in a leading to trailing edge direction. (C,C') E-Cadherin does not cluster within apical constrictions. (D) Centrosomes are arranged closely around apical constrictions. (anterior to the left, dorsal up).

3.2 The migratory pllp is a dynamic tissue

To assess whether cellular rosettes are units of tissue separation, I labeled *WT* embryos with the membrane marker BODIPY-ceramide (Cooper et al., 1999) and performed time-lapse analysis over a three-hour period. Individual rosettes were identified based upon apical membrane condensations, bottlenecked cell shapes and overall tissue organization. During tissue separation, the trailing cellular rosette including surrounding presumptive interneuromast cells reduced its migratory speed and lagged behind the pllp. During tissue separation, rosette cells and their surrounding presumptive interneuromast cells displayed elongated and stretched shapes which is in tune with pulling forces that are expected to act upon these cells during tissue separation. Importantly, tissue separation never occurred within rosettes. Instead, rosettes were separated exclusively in-between presumptive interneuromast cells (n=8 embryos analyzed). These observations demonstrate that cellular rosettes function as units of tissue separation (Figure 4).

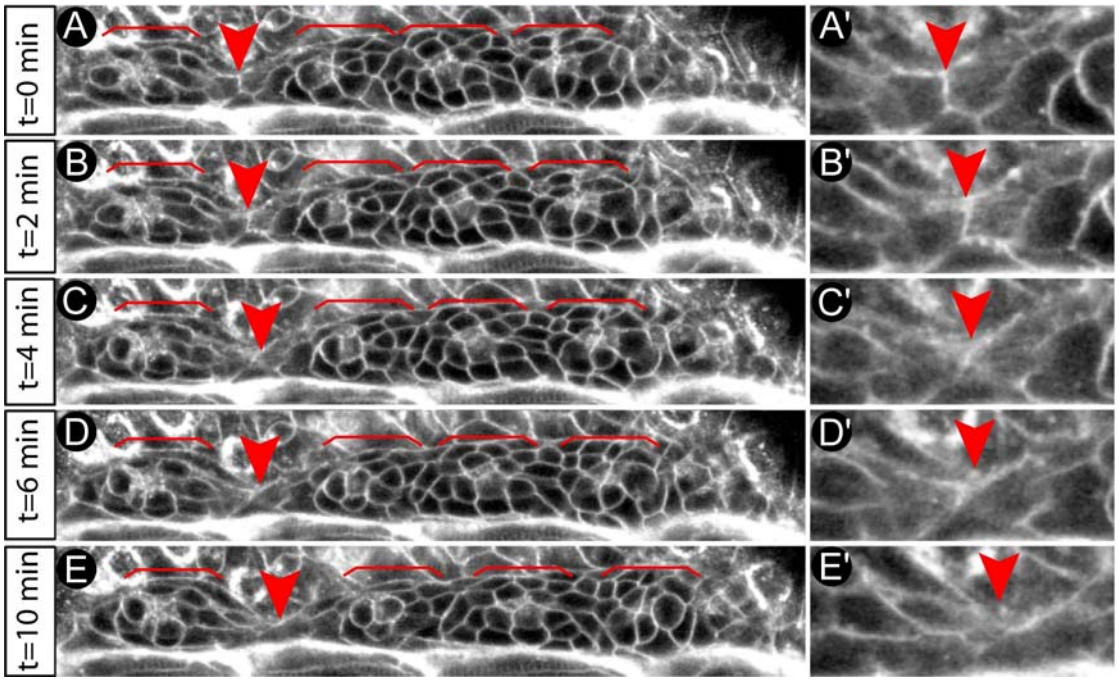

Figure 4: Dynamics of neuromast deposition. Shown is the process of neuromast deposition within a *WT* embryo that was labeled with the vital membrane marker BODIPY-ceramide and followed over a 10-minute period by time-lapse analysis. (A-E) Rosettes are indicated by red brackets and planes of tissue separation are indicated by red arrowheads. (A'-E') Details of cellular cell shape changes along the plane of tissue separation indicate that cells surrounding individual rosettes are extensively elongated and that tissue separation occurs in between them, which leaves individual rosettes intact. Therefore, rosettes including their surrounding cells are units of tissue separation. (anterior to the left, dorsal up).

Time-lapse and immunohistochemical analysis both suggested that apical focal points ensure increased affinity among rosette cells compared to cell-cell contacts between inter-neuromast cells. To test whether formation of apical focal points is indeed important for tissue morphogenesis and rosette separation, I decided to characterize mutants that affect cell polarity and apical junction

formation. For this purpose, I chose the zebrafish mutations *heart and soul* (*has*)/*prkci* and *penner*, which encodes the zebrafish homolog of Lethal giant larvae 2 (Lgl2). Both mutants affect cell polarity and epithelial maintenance (Horne-Badovinac et al., 2001; Peterson et al., 2001; Horne-Badovinac et al., 2003; Sonawane et al., 2005; Rohr et al., 2006).

The following sections describe *lgl2* gene expression and characterize Lgl2 and PRKCi involvement in pllp morphogenesis and pllo formation. Moreover, I will describe the involvement of the cell polarity regulator Nagie oko and the motor molecule Myosin VIa, in pllo formation.

3.3 Identification of Lgl1 and Lgl2 orthologs in zebrafish

To obtain the full-length sequence of *lgl2*, I performed homology searches using the annotated sequences of *Drosophila* and mouse *lgl2*. The full-length sequence (4287 base-pairs) was identified using the NCBI ENTREZ search engine (http://www.ncbi.nlm.nih.gov/entrez/), and the clone was obtained via RZPD (NCBI Gene ID: 321288 cDNA clone MGC: 55895 IMAGE: 3818830). (IMAGp998C239110Q3 Clone_ID=3818830). The protein encoded by zebrafish *lgl2* encodes a predicted 1020 amino acid protein with an expected molecular weight of 114 kD. Similarly, to obtain the *lgl1* sequence, I used the known mouse *lgl1* sequence (NCBI Gene ID: 16897) for a homology search of the Sanger Zv4.0 genomic sequence zebrafish database (http://www.ensembl.org/Danio_rerio/index.html). The sequence, obtained by assembling several sequence fragments (3166 base-pairs), encodes a predicted 1056 amino acid protein with an expected molecular weight of 116 kD. Alignments of the zebrafish Lgl proteins with Lgl orthologs, from other species, using “ClustalW” software (ver 1.83; http://www.ebi.ac.uk/clustalw) showed that zebrafish Lgl2 is highly conserved compared with mammalian Lgl2 (65% identity to both mouse and human Lgl2) and less conserved compared with the *Drosophila* ortholog (33% identity). Zebrafish Lgl1 is also highly conserved compared with mammalian Lgl1 (66% identity to both mouse and human Lgl1).

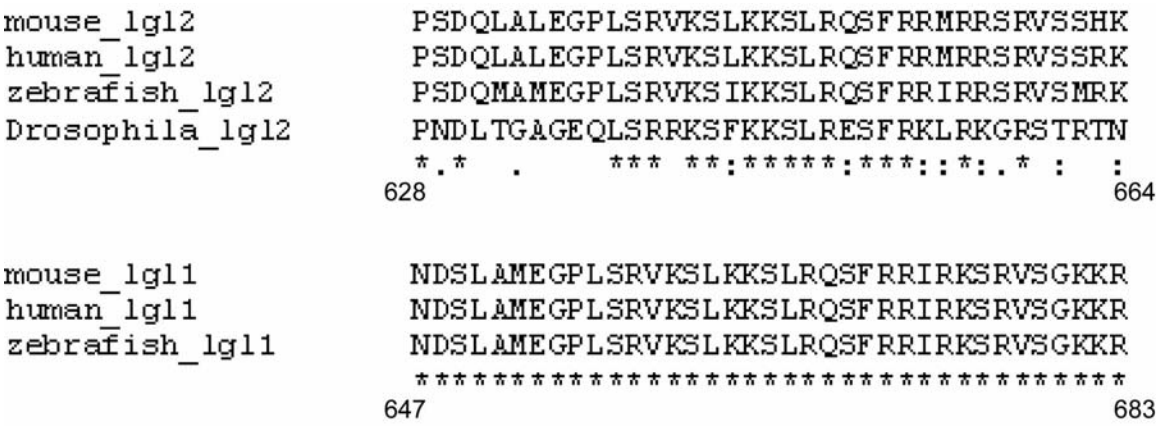

Figure 5: Conservation of Lgl between the different species. Amino acid sequence alignment of the zebrafish Lgls with orthologs from different species. The target site for Lgl phosphorylation, shows high amino acid identity to mammalian and *Drosophila* Lgl2 and complete sequence identity with mammalian Lgl1. (Identity indicated by asterisks, high similarity indicated by colons and low similarity indicated by dots. Numbers indicate the residue number of the zebrafish Lgls)

To analyze the functional and structural motifs of zebrafish Lgl2, I used the protein motif prediction tool “Simple Modular Architecture Research Tool” (SMART: http://smart.embl-heidelberg.de/). This analysis revealed that Lgl2 contains four WD40 repeats that are located within the N-terminal half of the protein. WD40 repeats are short ~40 amino acid motifs that frequently terminate in a Trp-Asp (w-d) di-peptide. WD-repeat proteins are found in all eukaryotes and have been implicated in a variety of functions. A common function of these proteins is to coordinate multi-protein complex assemblies.

3.4 Expression of *lgl2* within the migratory lateral line organ primordium

To characterize expression of both zebrafish *lgl* genes, I performed whole-mount in situ hybridization experiments on zebrafish embryos that were staged at the 4-cell stage, mid-blastula, mid-gastrula (50% epiboly), early to mid-somitogenesis (10-somite stage), 24 hpf, 36 hpf and 48 hpf. *lgl2* was maternally expressed at the 4 cell-stage (Figure 6A). At blastula stages (Figure 6B), *lgl2* was expressed in single interspersed cells. However, by 50 % epiboly, *lgl2* was ubiquitously expressed (Figure 6C). At the 10-somite stage, *lgl2* was strongly expressed throughout the entire head and within the bilateral otic placodes (Figure 6D). At 24 hpf, there was strong expression within the olfactory placode, the telencephalon and around the eye (Figure 6E). Most importantly for this study, by 36 hpf, *lgl2* was expressed ubiquitously with a strong expression in the migratory pllp and neuromasts of the posterior lateral line (see dots in Figure 6F). Finally, by 48 hpf, *lgl2* was strongly expressed within the head, gut, swim bladder, ear and neuromasts (Figure 6G). Moreover, *lgl2* expression levels were high within the secondary migratory pllp (Figure 6G').

In comparison, *lgl1* was also maternally expressed at the 4-cell stage (Figure 7A). During blastula stages and at 50% epiboly, *lgl1* was expressed ubiquitously throughout the embryo, albeit with different expression levels (Figure 7B,C). During the 10-somite stage, *lgl1* was strongly expressed throughout the head and along the embryonic midline (Figure 7D). At 24 hpf, *lgl1* was strongly expressed within the olfactory placode, the telencephalon and around the eye (Figure 7E). At 36 hpf, *lgl1* was ubiquitously expressed at high levels (Figure 7F). Expression at 48 hpf was strong in the cerebellum and in fin buds (Figure 7G).

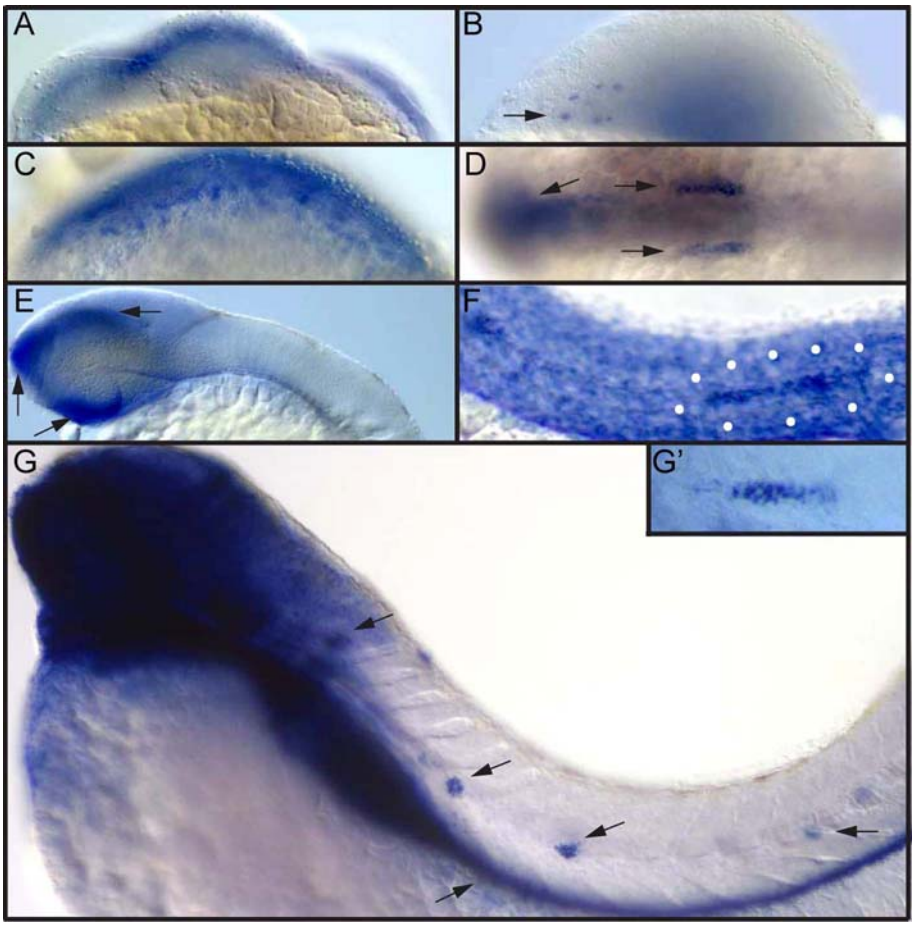

Figure 6: Expression pattern of zf-*lgl2* during different stages of embryogenesis. (A-C, face view) 4 cell stage (A), Blastula stage (B, arrows are indicating interspersed expression), 50% epiboly stage (C), (D-G, anterior to the left, dorsal up) 10 somite stage, dorsal view (D), 24 hpf, lateral view (E), 36 hpf, lateral view (F, dots outline the migrating pllp) and 48 hpf, lateral view (G and G').

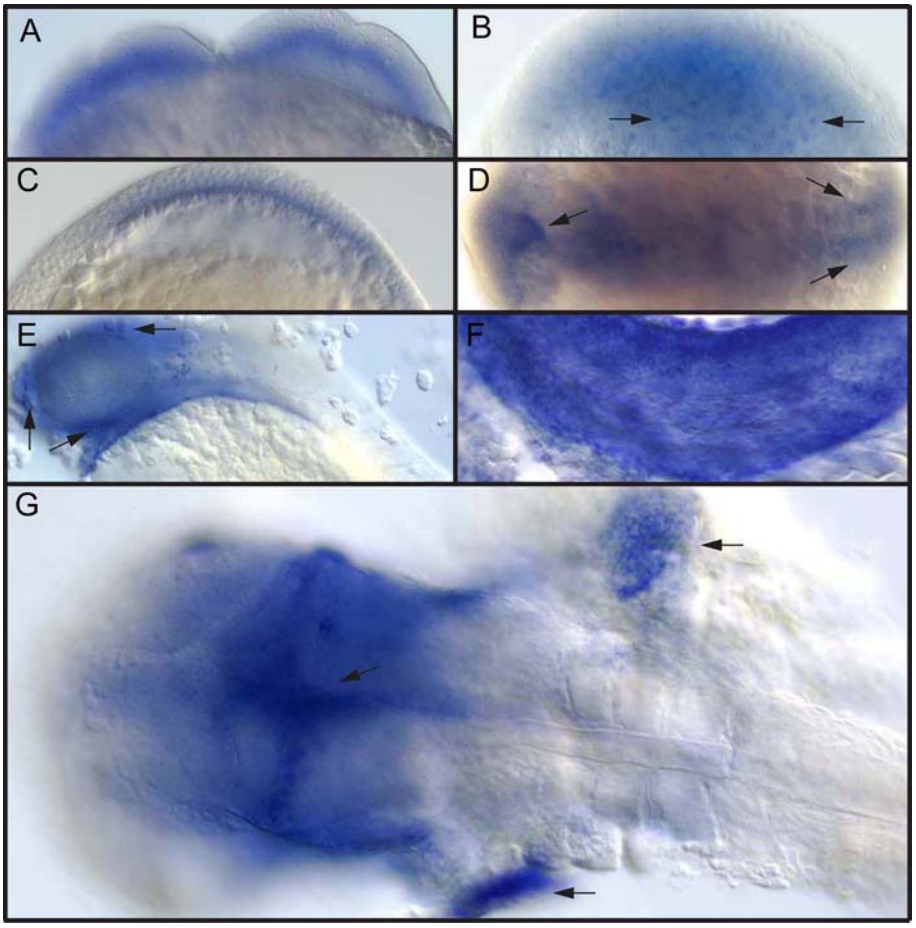

Figure 7: Expression pattern of *zf-lgl1* during different stages of embryogenesis. (A-C, face view) 4 cell stage (A), Blastula stage (B, arrows are indicating interspersed expression), 50% epiboly stage (C), (D-G, anterior to the left, dorsal up) 10 somite stage, dorsal view (D), 24 hpf, lateral view (E), 36 hpf, lateral view (F) and 48 hpf, dorsal view (G).

3.5 The pllo is affected in *lgl2* morphants

At 28-32 hpf, both *lgl2* (Figure 6F) and *has*/*prkci* (Figure 8, Hava et al., in preparation) displayed enriched expression levels within the pllp which suggested their involvement in pllp epithelial organization. Zygotic *penner*/*lgl2* mutants lack obvious defects prior to 72 hpf, presumably due to a strong maternal contribution (Sonawane et al., 2005).

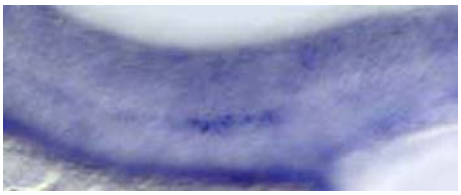

Figure 8: Expression pattern of *has/prkci* within the pllp. Expression pattern of *has/prkci* displays high levels within the pllp at 28-32 hpf (anterior to the left, dorsal up). Hava et al., in preparation.

To investigate the role of Lgl2 in neuromast formation, I designed three sequence-independent morpholino antisense oligonucleotides (MO), targeted to interfere with maternal translation. MOs are short (18-25bp) antisense oligonucleotides containing a modified sugar backbone (with a morpholine ring instead of ribose), which prevents degradation by exogenous RNA cleaving enzymes (RNases) or by metabolic degradation. In principle, MOs can be designed to interfere with the splicing of the pre-mRNA by blocking the splice donor or acceptor site at an exon/intron boundary and thus interfering with the correct processing of the mRNA or, alternatively, by binding to the 5' untranslated region (5'UTR) upstream of or including the ATG initiation site of translation. The latter MO design interferes with both maternal and zygotic mRNA translation, whereas interference with mRNA splicing only affects zygotic messages (Nasevicius and Ekker, 2000; Draper et al., 2001). All three ATG initiation site of translation targeting MO had a strong and comparable effect on pllo formation.

3.5.1 Efficacy of *lgl2* morpholino using a reporter and Lgl2 antibody

In order to check the efficacy of ATG directed MOs in blocking translation of Lgl2, I designed a reporter construct that expresses mRNA encoding eGFP-tagged Lgl2. The construct, *pCS2+14xUAS E1b lgl2:eGFP* was injected together with a *pB EF-1α Gal4-VP16* construct, which expresses the transcriptional activator Gal4-VP16 protein, which in turn binds to the Gal4-binding site (Upstream Activating Sequences, UAS) that drives the expression of Lgl2:eGFP (Koester and Fraser, 2001). These reporter constructs were co-injected together with $MO^{lgl2\text{-}atg}$, which binds to the 5'UTR including the ATG initiation site of translation, and which is the only MO that can bind completely to the exogenous reporter mRNA to block translation. Whereas most embryos injected with the reporter construct strongly expressed the membrane-associated fusion protein (n=27/35), Lgl2:eGFP expression was absent in all embryos co-injected with $MO^{lgl2\text{-}atg}$ (n=0/32) (Figure 9). Another way of confirming the efficacy of the MOs is by immunohistochemical staining with an antibody against Lgl2 (donated by M. Sonewane, Tubingen). For this purpose, any of the three *lgl2* MOs could be used, since all three of them block the translation of endogenous mRNA. Immunohistochemical stainings of 32 hpf *lgl2* morphants revealed a strong reduction of Lgl2 expression (Figure 10).

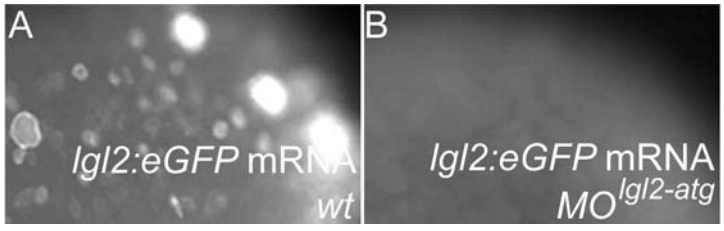

Figure 9: Efficiency of *lgl2* morpholino. Injection of a reporter expressing construct, encoding Lgl2:eGFP results in strong protein expression during gastrula stages in *WT* (A) but is efficiently blocked in $MO^{lgl2\text{-}atg}$ injected animals (B).

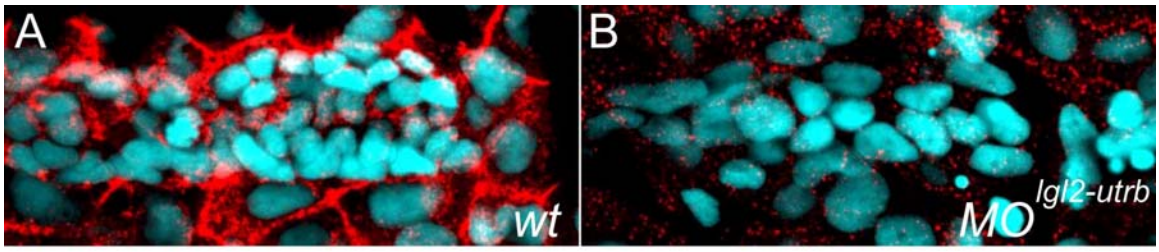

Figure 10: Efficacy of the $MO^{lgl2\text{-}utrb}$. Immunohistochemical analysis reveals that endogenous Lgl2 levels (red) are strongly depleted within the 32 hpf primordium of $MO^{lgl2\text{-}utrb}$ injected animals (B) compared to *WT* (A). (anterior to the left, dorsal up).

3.5.2 Neuromast deposition is affected in *lgl2* morphants

In order to quantify the effect of knocking down *lgl2* on the pllo, I performed whole mount In-situ hybridization using *eyes absent 1* (*eya1*) probe, as a marker, which is expressed within the migrating primordium as well as in deposited neuromasts (Sahly et al., 1999). Quantification of neuromast number revealed that *WT* embryos had between 8 to 9 *eya1* positive neuromasts at 48 hpf, the time by which all neuromasts have been deposited by the first migrating primordium (Figure 11 A). Each of the three MOs targeting the initiation site of translation gave a dosage-dependent reduction in *eya1* positive neuromast number (Figure 11 B). Moreover, neuromasts were found to be progressively sparser towards the posterior half of the embryo compared to the *WT*, indicating that either the pllp had failed to complete migration into the tail or that deposition of neuromasts from the pllp was impaired more strongly at later stages. These results indicate that Lgl2 is necessary for neuromast formation in the pllo.

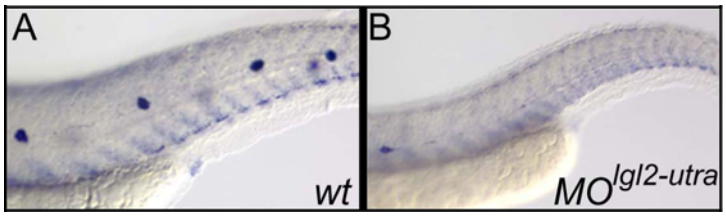

Figure 11: *lgl2* morphants lack neuromasts in pllo. Expression of the neuromast marker *eya1* at 48 hpf in *WT* animals (A). In $MO^{lgl2\text{-}utra}$ morphant (B) a sever reduction in neuromast number (anterior to the left, dorsal up)

3.5.3 *PRKCi*, *nok* and *myosinVIa* morphants resemble the *lgl2* morphant pllo phenotype

As described previously, *heart and soul* (*has*)/*prkci* affects cell polarity and epithelial maintenance (Horne-Badovinac et al., 2001). Moreover, *has*/*prkci* displays enriched expression levels within the pllp. Therefore, I analyzed the effect, of PRKCi deletion, on pllo formation. Like *penner* mutants, *heart and soul* (*has*)/*prkci* zygotic mutants also lack defects in neuromast formation, probably due to maternal mRNA contribution. Therefore, I used MOs designed to intefere with maternal mRNA *has*/*prkci* translation. Injection of *prkci* MO resulted in a dosage-dependent reduction in *eya1* positive neuromast number (Figure 12).

nok mutants exhibit pigmentation defects, abnormal brain and body shape and circulation defects, which resemble *has* mutants (Wei and Malicki, 2002). Therefore, I tested whether knocking down *nok* would have an effect on pllo formation comparable to knock down of *prkci* or *lgl2*. Injection of *nok* MO was also found to result in reduction of *eya1* positive neuromasts number, although the effect was not as severe as loss of *prkci* or *lgl2* (Figure 12). This result indicates that *nok* could be involved in the formation of the pllo, which could be compensated by the activity of other molecules, also involved in the formation of the pllo.

Another protein that is known to interact with Lgl2 in *Drosophila* neuroblasts is Myosin VI (myo VI), which is involved in the regulation of asymmetric division of the neuroblast (Petritsch et al., 2003). In addition, myo VI is essential for *Drosophila* border cell migration (Geisbrecht and Montell, 2002). To investigate whether myo VI also has a role in pllo formation, I used *myo VI* MOs for a knock down. In zebrafish, two isoforms of *myoVI* (*myo VIa* and *myo Vib*) are present, therefore I injected ATG directed MOs, that target either *myosin VIb* or *myosin VIa* (Kappler et al., 2004). *myosin VIa*, which is broadly expressed (Seiler et al., 2004), resulted in a dosage-dependent reduction of *eya1* positive neuromast number that was as severe as the loss of neuromasts, observed in *lgl2* or *prkci* morphants (Figure 12). Similar to Lgl2 and PRKCi, myo VIa also shows involvement in the formation of the pllo.

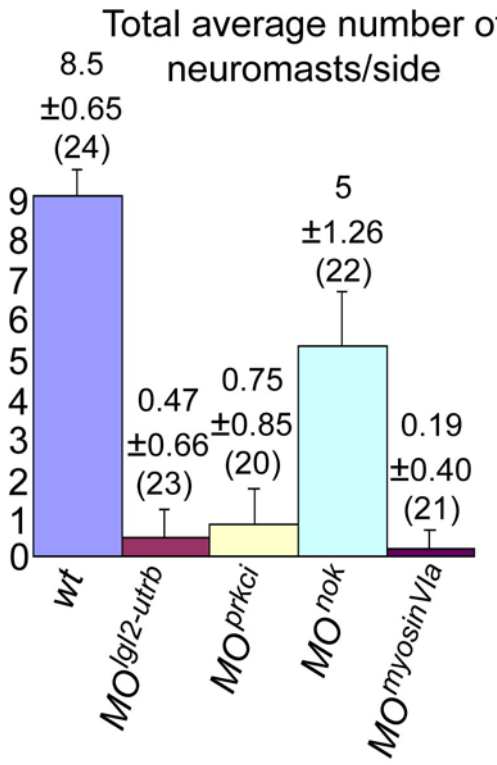

Figure 12: Effect of the different morpholinos on the pllo formation. Quantification of average number of neuromasts/body side ± standard deviation and the total number of animals counted (brackets) are shown for the different morphants.

3.6 Specificity of MOs directed againts *lgl2*, *PRKCi* and *nok*

The specificity of $MO^{lgl2\text{-}utrb}$, MO^{prkci} and MO^{nok} was tested by co-injection of synthetic and non-complementary *lgl2*, *prkci* or *nok* mRNAs encoding amino-terminal HisMyc-tagged fusion proteins together with $MO^{lgl2\text{-}utrb}$, MO^{prkci} or MO^{nok} respectively. In all cases, a rescue of neuromasts number was observed usually on one side of the embryo, presumably due to a mosaic expression of the rescue mRNAs (Figure 13). Given these results, the defects in pllo formation, observed after injection of either MOs ($MO^{lgl2\text{-}utrb}$, MO^{prkci} and MO^{nok}), are likely to be a result of knocking down either one of the three genes. Since mRNA encoding myo VIa was not available, I could not confirm the specificity of the phenotype observed by $MO^{myosinVIa}$ injection.

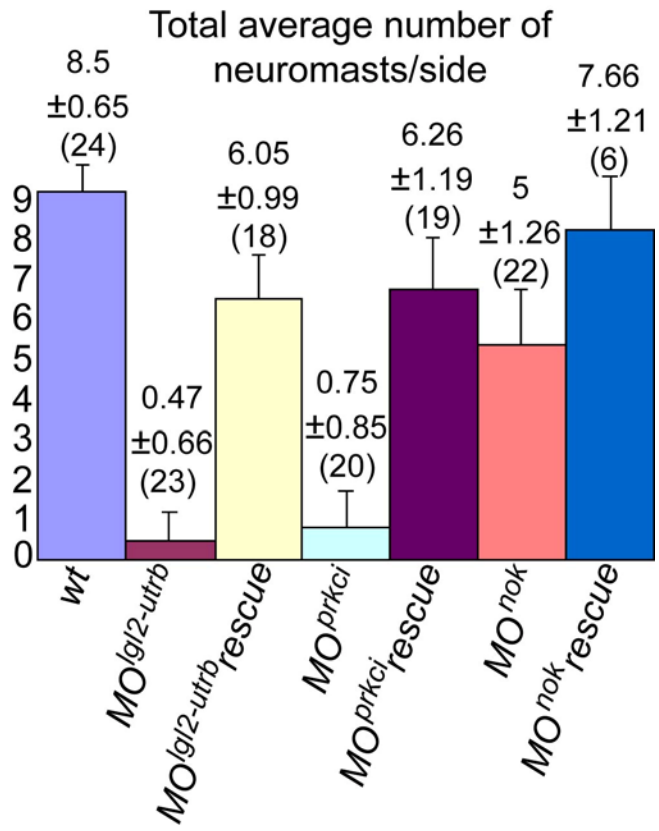

Figure 13: Specificity of the different morpholinos. Quantification of average number of neuromasts/body side ± standard deviation and the total number of animals counted (brackets) are shown for the different backgrounds.

3.7 Lgl2 phosphorylation by PRKCi affects pllo formation

In a variety of cellular contexts, PRKCi regulates Lgl2 function by phosphorylation events within the central Lgl2 domain of the protein, which render Lgl2 inactive (Betschinger et al., 2003; Plant et al., 2003; Yamanaka et al., 2003). In order to investigate whether phosphorylation of Lgl2 by PRKCi is essential in the context of pllo formation, I used site-directed mutagenesis to generate a non-phosphorylatable form of Lgl2, $Lgl2^{S5A}$ (constitutively active) in which Serines (643, 647, 651, 658 and 661) within the central Lgl target domain were changed to Ala. As a control, a phosphomimetic form of Lgl2, $Lgl2^{S3E}$

(autoinhibitory form) carrying changes of Serines (643, 647 and 651) to Glu, was used. Finally, a dominant inhibitory form of PRKCi (kinase dead), $PRKCi^{KD}$, in which the residues Pro 408 and Glu 409 within the catalytic center are exchanged for Ala (Rohr et al., 2006), was used. Over-expression of either $Lgl2^{S5A}$ or $PRKCi^{KD}$ in *WT* gave a dominant effect with reduced number of neuromasts, usually on one side of the embryo, presumably due to mosaic protein expression (Figure 14). In contrast, over expression of the auto-inhibitory form, $Lgl2^{S3E}$, had no effect on neuromast formation. These results suggest that Lgl2 phosphorylation by PRKCi is essential in the context of pllo formation.

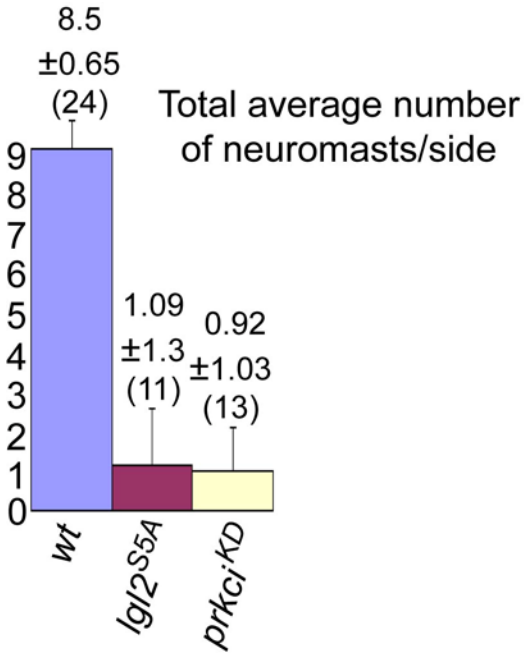

Figure 14: pllo formation is affected by presumably antagonistic activities of Lgl2 and PRKCi. Quantification of average number of neuromasts/body side ± standard deviation and the total number of animals counted (brackets) are shown as a consequence of over expressing mutant Lgl2 proteins, within *WT* embryos.

3.8 Apical membrane constriction and rosette formation is regulated by *lgl2* and *prkci*

Next, I assessed epithelial organization and rosette formation within the pllp, of animals knocked-down for *lgl2*, *prkci*, or animals over-expressing $lgl2^{S5A}$ or $prkci^{KD}$ mRNAs. A change in the pllp morphogenesis of either of these animals compared with *WT* pllp, may explain the defects in pllo formation, observed in these animals. Since ~8.5 ng of $MO^{lgl2\text{-}utrb}$ resulted in a significantly reduced size of the placode (see section 3.11) from which the pllp delaminates, lower concentrations (~5-6 ng) of the MO were injected, in order to generate hypomorphic conditions and to gain a normal sized pllp. Similar to the loss of Lgl2 or PRKCi, embryos overexpressing mutant forms of the proteins displayed a reduced number of cellular rosettes based on the lack of actin, ZO-1 and PRKCs positive focal points (Figure 15C-J). Generally, in pllps with one rosette, the rosette was located at the trailing end of the pllp, whereas the central region, like the leading edge of the pllp, contained actin rich spots, probably due to a delay in rosette formation (Figure 15C',I', H, Figure 17). Actin, PRKC and E-Cadherin were localized along all cell membranes, whereas ZO-1 was not detectable. Lack of rosette formation coincided with a failure of cells to acquire bottle-necked shapes, to translocate nuclei to one side and to arrange centrosomes close to the opposite side (Figure 16D,F, H, J), altogether indicating that the cells within the pllps are impaired in their ability to polarize. Therefore, reduced activity of Lgl2 or PRKCi results in a severe delay or complete failure of pllp cells to constrict apical membranes, acquire bottlenecked shapes and to arrange into cellular rosettes.

Using lower concentrations of the MOs resulted in a reduced number of neuromasts at 32 hpf (Figure 18), indicating that neuromast formation is correlated with rosette formation within the pllp and that a failure to form rosettes results in a failure to form neuromasts.

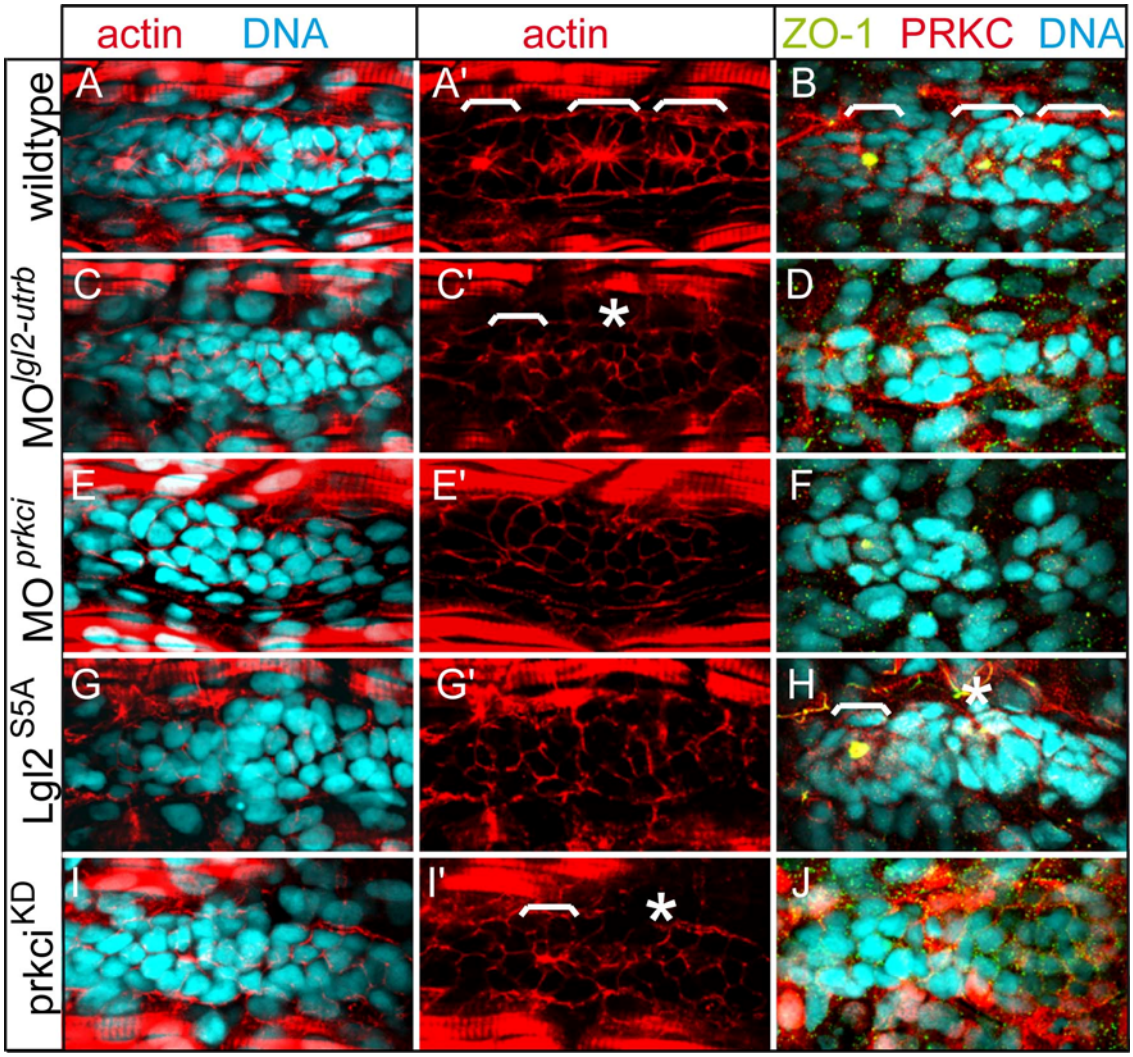

Figure 15: Apical membrane constriction and rosette formation is affected by antagonistic activities of Lgl2 and PRKCi. Epithelial organization of pllp cells was assayed by immunohistochemistry. Shown are reconstructions of confocal images of the pllp at 36 hpf. The number of rosettes (white brackets) is strongly reduced within different backgrounds. (C', I') Instead, the central region of the pllp frequently contains actin rich spots, which are indicative of incomplete apical constriction (white asterisks). (D,F,J) Loss of ZO-1 expression within severely affected pllps that fail to produce rosettes. (J) Note mosaic and strong ectopic expression of PRKCi^{KD} upon overexpression. (anterior to the left, dorsal up).

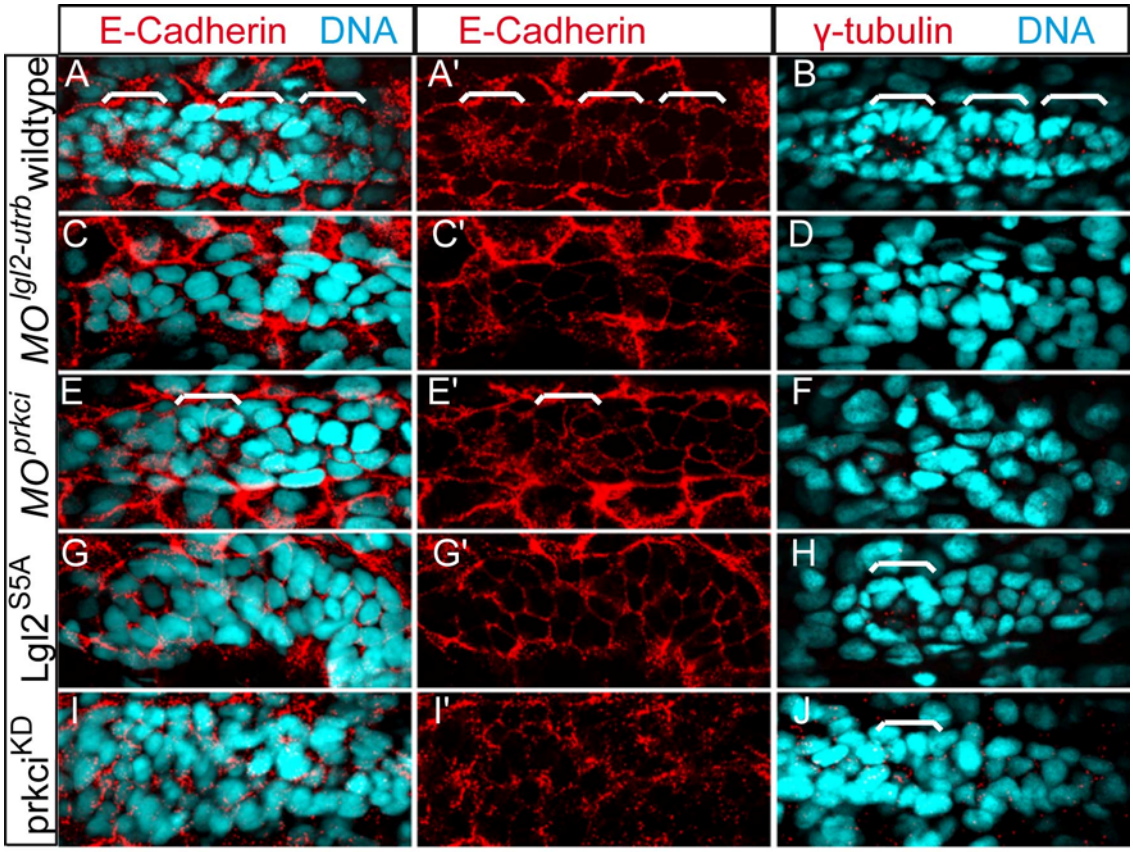

Figure 16: Apical clustering of centrosomes and rosette formation is affected by antagonistic activities of Lgl2 and PRKCi. Epithelial organization of pllp cells was assayed by immunohistochemistry. Shown are reconstructions of confocal images of the pllp at 36 hpf. In the wild type 3 rosettes are formed within the pllp (A-B, white brackets), whereas in the different backgorouds it is strongly reduced (C-J). E-Cadherin is widely expressed along all cell membranes(C,E,G,I). Lack of rosette formation corresponds with a failure of centrosomes to arrange apically (D,F,H,J). (anterior to the left, dorsal up).

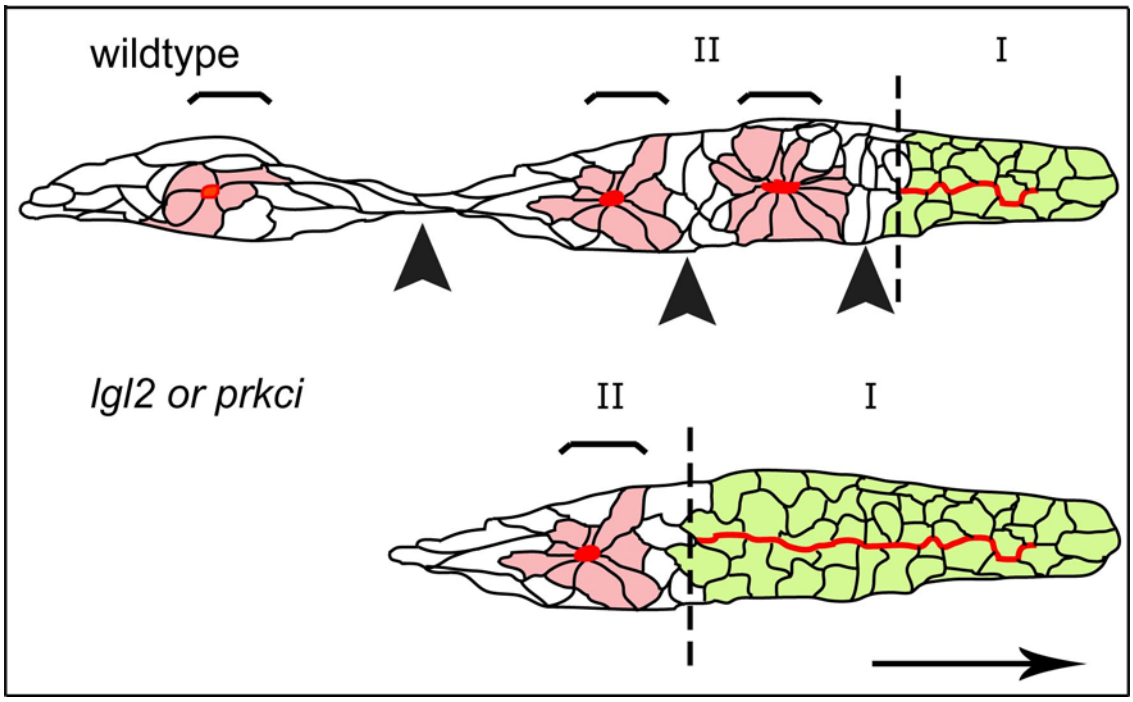

Figure 17: Schematic diagram of tissue separation within the pllp. Red indicates the distribution of actin rich apical membranes, which are widely present within the leading edge region of the pllp (green cells, region I) and confined to apical focal points within rosettes (light red cells, region II; regions indicated by dotted line), which are surrounded by interneuromast cells (white cells). In *lgl2* or *prkci* morphants, the process of rosette formation is delayed. Brackets demarcate presumptive neuromasts and black arrowheads indicate future points of tissue separation. The direction of pllp migration is indicated by black arrows. (anterior to the left, dorsal up).

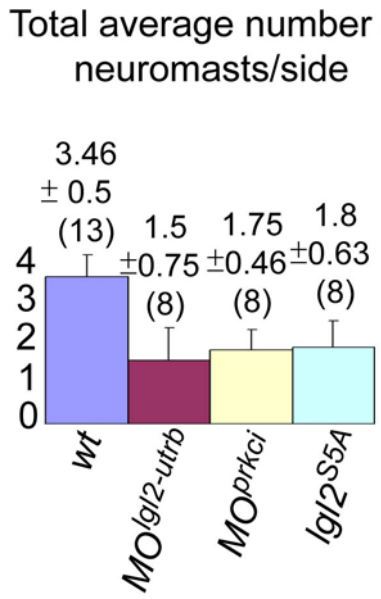

Figure 18: Neuromast deposition 36 hpf in wild type and hypomorphic animals. Quantification of average number of neuromasts/body side ± standard deviation and the total number of animals counted (brackets) are shown for the different backgrounds

3.9 Loss of Lgl2 does not affect Delta D expression although junction structure is altered

One mechanism by which Lgl2 and PRKCi may disrupt epithelial rosette formation is via affecting the Delta/Notch pattern, which underlies hair cell progenitor and support cell formation within presumptive neuromasts (Itoh and Chitnis, 2001; Ghysen and Dambly-Chaudiere, 2004). Delta/Notch signaling between hair cell progenitors and surrounding support cells pre-patterns the pllp prior to neuromast deposition (Itoh and Chitnis, 2001). To test this possibility, I characterized hair cell progenitor distribution within the pllp using an antibody against Delta D and assessed rosette formation using antibodies against PRKC or β-catenin. In *WT*, Delta D immunoreactivity was confined to one or two presumptive hair cells within each rosette. Delta D-positive aggregates associated with but did not co-localize with apical focal points (Figure 19A,B).

Three-dimensional reconstructions of confocal z-stacks revealed that the nuclei of Delta D-positive presumptive hair cells are positioned beneath each apical focal point. This correlation suggests that presumptive hair cells may provide a necessary cue for apical constriction.

To test the possibility that failure of rosette formation could be due to a lack of hair cell progenitors, I analyzed Delta D expression in *lgl2* morphants. Embryos injected with $MO^{lgl2\text{-}utrb}$ contained Delta D-positive hair cell progenitors, which demonstrates that hair cell specification does not require Lgl2. However, in contrast to *WT*, hair cell progenitors were often associated with larger clusters of several presumptive neuromasts that failed to separate (n=10/37 [27%]; Figure 19C). In rare events, hair cell progenitors were also found in regions of the pllp that lacked apical membrane constrictions (n=2/37 [5.4%]; Figure 19D). These findings suggest that Lgl2 is required for formation of apical focal points and rosette clustering rather than for controlling Delta/Notch-mediated hair cell specification.

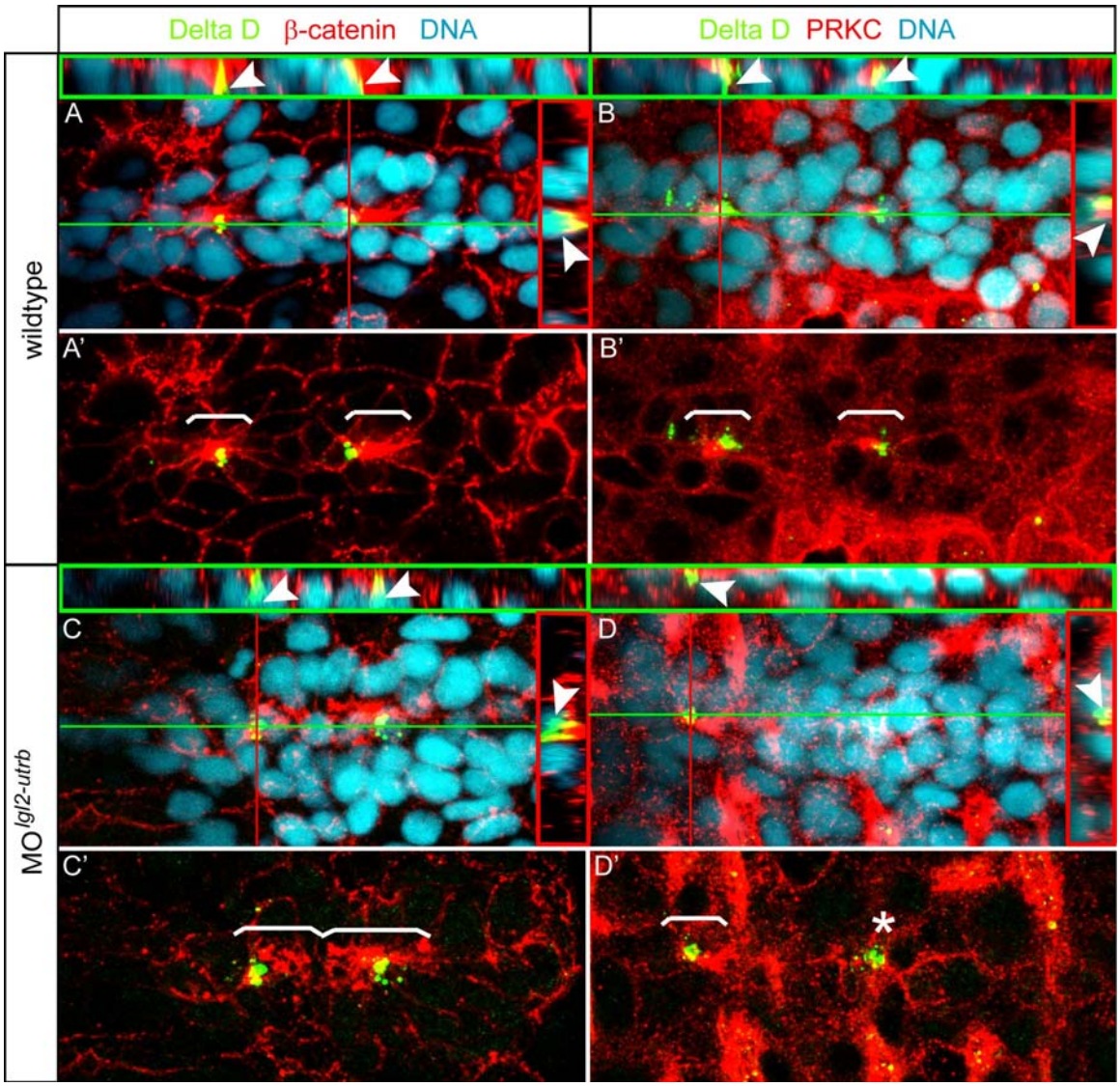

Figure 19: Loss of Lgl2 affects separation of Delta D positive hair cell progenitors within the pllp. Epithelial organization of pllp cells was assayed by immunohistochemistry. Shown are reconstructions of confocal images of the pllp at 36 hpf. (A-D) Red lines indicate cross section planes, green lines sagital section planes and the respective sections are shown within red (apical to the right) or green insets (apical to the top). White brackets indicate position of individual rosettes. (A,B) In *WT*, individual rosettes contain apical β-catenin and PRKC positive focal points that are associated with Delta D. White arrowheads (red and green insets) indicate Delta D positive aggregates that are associated with apical constrictions but extend more basolateral. (C) Example of an *lgl2* morphant pllo with incomplete separation of two

rosettes (two white brackets). (D) Example of an *lgl2* morphant presumptive Delta D-positive hair cell that is not associated with a rosette (white asterisk). (anterior to the left, dorsal up).

3.10 Cell proliferation within the pllp

Loss of cell polarity could result in uncontrolled cell proliferation (Bilder et al., 2000; Wodarz A., 2000; Bilder, 2004). Therefore, I investigated whether the proliferation rate within the migrating pllp is changed in *lgl2* morphants compared with *WT* embryos. Proliferation was assessed at 32 hpf by a BrdU incorporation assay, counterstained with DAPI on wild type, *lgl2* morphants and *nok* morphant embryos (I also performed this assay on *nok* morphants since knocking-down *nok* resulted in a phenotype which resembles the hypomorphic *lgl2* phenotype (see section 3.5.3)). The proliferation rate within *lgl2* and *nok* morphant pllps was higher than within *WT* embryos (Table 1. and Figure 20). Moreover, in *WT* pllp proliferation takes place mainly in the leading edge of the pllp, where cells are not organized into rosettes, whereas in the trailing end of the pllp, proliferation is reduced, indicating that polarized cells that commit themselves to be part of the future neuromast arrest proliferation. In the *lgl2* morphant pllp, on the contrary, cells undergo proliferation throughout the entire pllp, indicating that the cells fail to commit themselves to be part of a future neuromast and to slow down proliferation.

Genotype (number of embryos)	% Proliferation	Number of BrdU/DAPI
Wild type (5)	54.124	28.4/52.6
lgl2 morphants (5)	67.448	32.9/48.8
nok morphants (5)	66.256	12.9/19.6

Table 1: Brdu and nuclear counterstaining reveal higher proliferation rate in *nok* or *lgl2* morphant pllps. Quantification of average numbers of percentage of BrdU positive cells relative to Dapi counter-stained cells/pllp at 36 hpf, and average of absolute numbers of BrdU positive cells and Dapi counter-stained cells/pllp. The total number of animals counted (brackets) is shown for the different backgrounds.

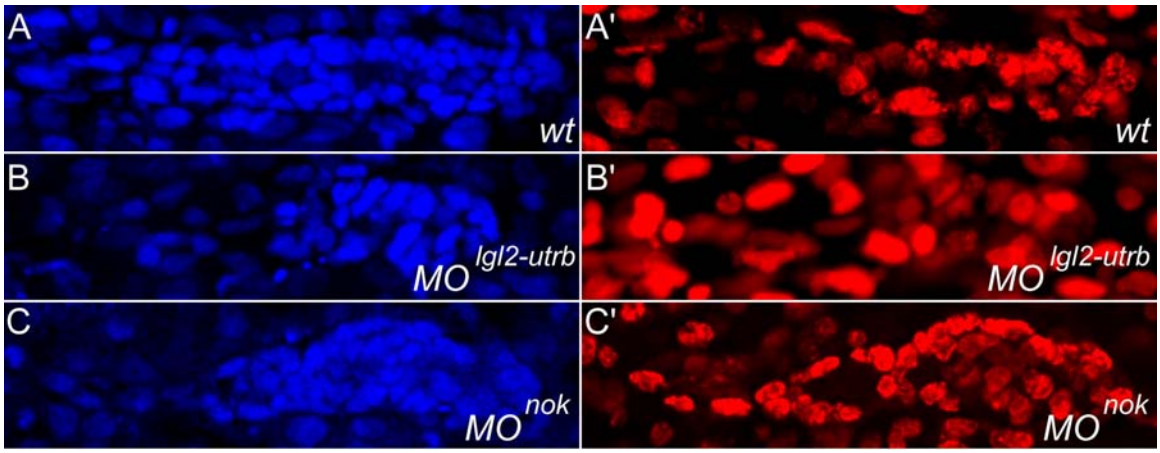

Figure 20: Brdu and nuclear counterstaining show a higher proliferation rate in morphants. Proliferation rate assayed by BrdU injection and immunohistochemistry. Shown are confocal images of the pllp at 36 hpf for different genetic backgrounds. *WT* with nuclear staining (A) and BrdU staining (A'), $MO^{lgl2\text{-}utrb}$ injected animals with nuclear staining (B) and BrdU staining (B') and MO^{nok} injected animals with nuclear staining (C) and BrdU staining (C'). (anterior to the left, dorsal up).

3.11 Placode size is reduced in *lgl2* morphants

Defects in neuromasts formation could be due to reduced cell number within the migrating pllp. During development of the pllo, the pllp delaminates from a placodal tissue, which is positioned posterior to the ear (Metcalfe, 1985). In order to check whether the effect on the pllo formation results from reduction in placodal size, whole mount in-situ hybridization was performed using *eya1* to estimate the placode size at 20 hpf. At high $MO^{lgl2\text{-}utrb}$ concentrations (~8.5 ng),

the placodal size of the *lgl2* morphants was reduced compared with *WT* (Figure 21 A, B). This finding was confirmed by determining cell count (Figure 21 C). This result indicates that in case of the amorphic phenotype, where Lgl2 is strongly reduced, lack of neuromast formation strongly correlates with reduced cell number in the migrating pllp.

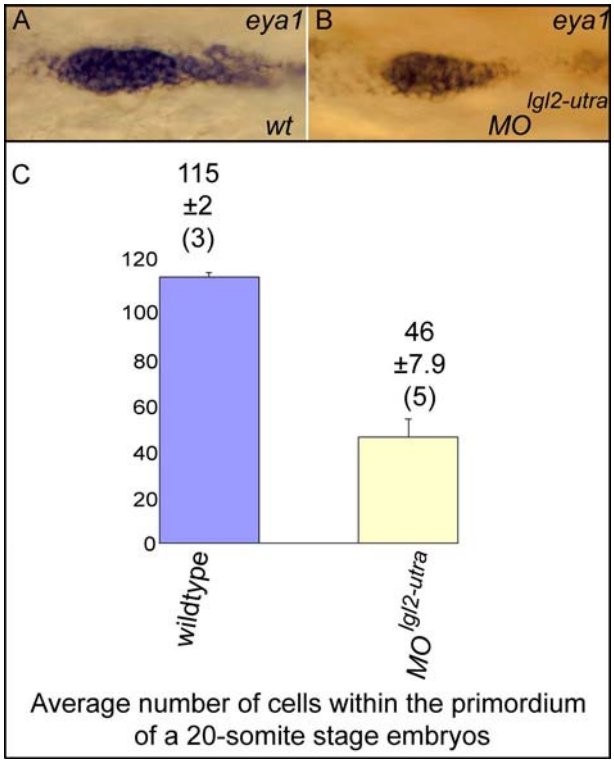

Figure 21: Size reduction of the placode of the posterior lateral line at 20 hpf. Expression of eya1 at 20 hpf marks the posterior placode from which the pllp delaminates. Loss of Lgl2 results in a smaller placode prior to the onset of pllp migration (A,B). Quantification of average numbers of cells/pllp ± standard deviation at the 20-somite stage. The total numbers of animals counted (brackets) are shown for *WT* and *MO*$^{lgl2\text{-}utra}$ injected animals (C).

3.12 Analyzing the migration of the pllp

Lgl2 has been implicated in directional cell migration. During oogenesis of the *Drosophila lgl2* mutant egg, follicle cells fail to complete migration (De Lorenzo et al. 1999). To assess whether lack in neuromast formation, in *lgl2* morphants, could be a result of a failure of the pllp to migrate properly, I performed the following experiments:

3.12.1 The pllp migration speed is reduced in *lgl2* morphants

Lack of neuromast formation in the *lgl2* morphants could be the result of a failure of the pllp to migrate to the tip of the tail. To investigate whether this is the case, *WT* fish and *lgl2* morphants were labeled with BODIPY-ceramide (Cooper et al., 1999), which marks the cell membrane, and the speed of the migrating pllp was analyzed by visual inspection under confocal microscope over an 8 hour period, between 32 to 40 hpf. The pllp localization was defined by somite position and the speed was calculated as somites/ hour. The speed of morphant pllps was reduced (1.4±0.2 somites/hour, n=3) compared with the speed of *WT* pllps (2.6±0.1 somites/hour, n=4). Nevertheless, most *lgl2* morphant pllps reached the tip of the tail. Thus, the velocity of the pllp in the *lgl2* morphant, is reduced but not completely inhibited. Important to mention that in contrast to *sdf1* morphant pllps, *lgl2* morphant pllps migrate straight along the stereotyped migration path (David et al., 2002; Li et al., 2004; Haas and Gilmour, 2006).

3.12.2 Evidence for a cell autonomous role of Lgl2 during cell migration of the pllp

Cell autonomy of a gene refers to a case in which this gene acts solely within the cell, without altering other cells or being affected by the genotype of other cells. It is an intriguing question whether *lgl2* functions cell autonomously during the migration of the pllp. In order to check this, I transplanted cells from *WT* or *lgl2*-injected blastula stage donors into *lgl2*-injected or *WT* blastula stage hosts, respectively. I expected that, if *lgl2* affects cell migration speed autonomously, a greater percentage, of *lgl2*-deficient cells transplanted into *WT* hosts, is predicted to be located to the trailing end of the pllp, when compared to control experiments in which *WT* cells are transplanted into *WT* host tissue. Conversely, more *WT* cells are predicted to be located to the leading edge of *lgl2* morphant pllps.

In the experiments in which the donor was *WT* and the host was *lgl2* morphant, most *WT* cells within the migrating primordium migrated faster than the *lgl2* morphant cells, and localized mostly at the leading edge of the pllp (Table 2, Figure 22B). In the reciprocal experiments, most morphant cells localized in the middle of the pllp or at the trailing end (Table 2, Figure 22C). In a control experiment in which *WT* donor cells were transplanted into *WT* acceptor embryos, cells showed equal distribution within the pllp compared to the other two cases, with a tendency of the donor cells to localize more to the leading edge (Table 2, Figure 22A). These results indicate that *lgl2* may function cell autonomously during the migration of the pllp. However, the differences seen could not be analyzed statistically due to the small number of successful experiments, and the number of data sets available for analysis could not be increased due to technical limitations in producing animals with mosaic pllp.

Donor/Acceptor	Anterior (leading)	Middle	Posterior (trailing)
wt/wt (2)	8 cells ± 7.07	6.5 cells ± 6.36	3.5 cells ± 0.7
wt/*lgl2* morphant (6)	4.1 cells ± 2.22	2.5 cells ± 3.33	0.6 cells ± 1.63
lgl2 morphant/wt (4)	1.75 cells ± 2.21	3.5 cells ± 1.91	3.25 cells ± 2.21

Table 2: Genetic mosaic analysis in the pllp. Quantification of average numbers of cells/pllp-domain ± standard deviation at 32 hpf for 3 different pllp domains. The total number of animals counted (brackets) is shown for different types of experiments.

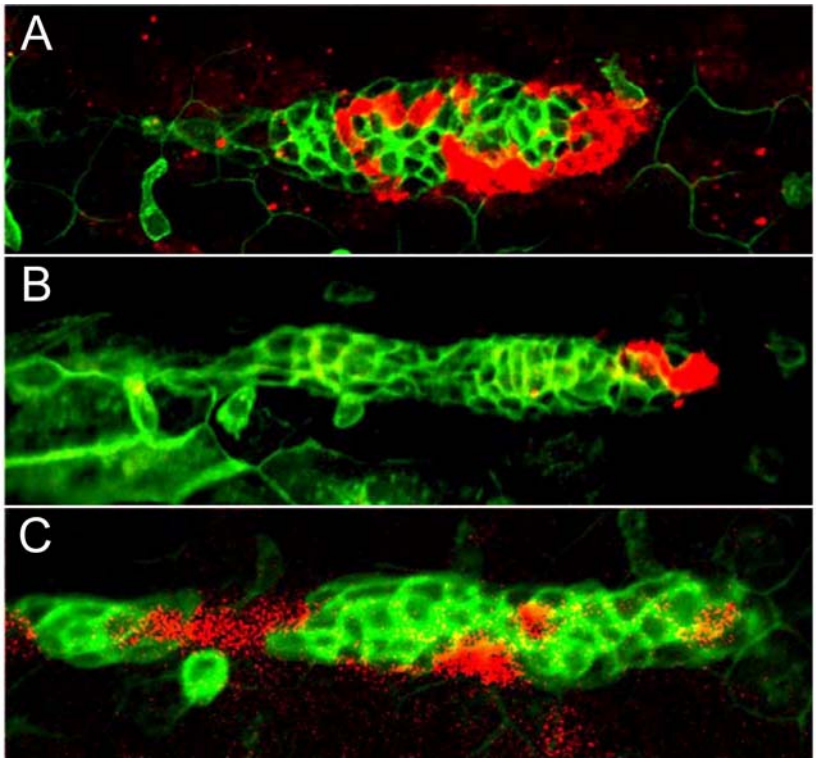

Figure 22: Genetic mosaic analysis in the pllp. *WT* cells marked with rhodamine dextran (Red) transplanted into wt *Tg(cldnB:GFP)* (green) host (A), *WT* cells marked with rhodamine dextran (Red) transplanted into $MO^{lgl2\text{-}utrb}$ injected *Tg(cldnB:GFP)* (Green) host (B) and $MO^{lgl2\text{-}utrb}$ injected cells marked with rhodamine dextran (Red) transplanted into *Tg(cldnB:GFP)* (Green) host (C) (anterior to the left, dorsal up).

3.12.3 Myosin II is essential for pllp migration

Several studies have indicated a role for non-muscle myosin II (MyoII) in cell migration (Nakayama et al., 2005; Schaar and McConnell, 2005; Koppen et al. 2006). Inhibition tests, using blebbistatin, a specific MyoII inhibitor, revealed that MyoII inhibition generally resulted in suppression of cell migration, though this was not true in all cell types examined (Nakayama et al., 2005). Blebbistatin inhibits the ATPase activity of MyoII by binding to the ATPase intermediate with ADP and phosphate bound, thus slowing down release of phosphate, but does not interfere with myosin light chain kinase activity of Myo II (Straight et al., 2003; Kovacs et al., 2004). Since Lgl2 is known to be associated with a MyoII heavy chain (Strand et al., 1994, Kalmes et al., 1996), I used blebbistatin to assess the potential involvement of Myo II in pllo formation. At 48 hpf, after neuromast deposition, blebbistatin-treated embryos, displayed disturbed pllp migration, resulting in reduced neuromast formation when compared with un-treated sibling embryos. The results differed strongly between individual embryos, since pllp migration-defects changed from one embryo to the other, resulting in a large variation in neuromast deposition and consequently high standard deviation (Figure 23). Nonetheless, it seems likely that Myo II is involved in the regulation of pllp migration, since all pllps failed to complete migration to the tip of the tail.

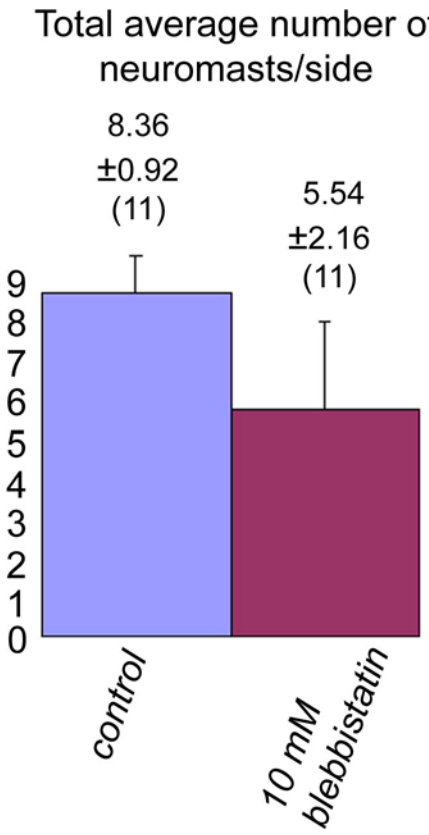

Figure 23: Myosin II involvement in pllp migration, affect pllo formation. Quantification of average number of neuromasts/body side ± standard deviation and the total number of animals counted (brackets) are shown for wild type and animals treated with blebbistatin.

3.13 Lgl2 does not affect Met receptor tyrosine kinase signaling in the proximal part of the migratory pllp

Another possible mechanism by which Lgl2 may disrupt epithelial rosette formation is via affecting the Met receptor tyrosine kinase signaling pathway. Down-regulation of *met*, a marker for migratory cell types, within the proximal part of the pllp has been implicated in the periodic deposition of neuromasts (Haines et al., 2004). Altered *met* expression within the proximal part of the *lgl2*

morphant-pllp could result in mis-deposition of neuromasts. To investigate this possibility, *met* expression was tested by in situ hybridization. Indeed, the expression pattern of *met* in both *WT* and *lgl2* morphants was comparable and *met* was down-regulated within the trailing region of both primordiums, indicating that the Met-regulated deposition of neuromasts is not changed and that rather the mechanism discussed in section 3.9, which is critical for neuromast formation, is affected in the morphants (Figure 24).

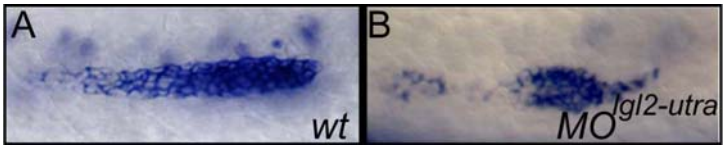

Figure 24: Downregulation of *met* expression at the trailing end of the pllp is not affected in *lgl2* morphants. (A,B) *met* expression at 32 hpf is diminished within the trailing end of *WT* and MO^{lgl2} pllps demonstrating that the stop mechanism for presumptive neuromasts is still functional upon loss of Lgl2. (anterior to the left, dorsal up).